Geochemistry Geophysics Geosystems G3
AN ELECTRONIC JOURNAL OF THE EARTH SCIENCES
Published by AGU and the Geochemical Society

Article
Volume 8, Number 7
26 July 2007
Q07010, doi:10.1029/2007GC001601
ISSN: 1525-2027

Two-dimensional numerical models of open-top hydrothermal convection at high Rayleigh and Nusselt numbers: Implications for mid-ocean ridge hydrothermal circulation

Fabrice J. Fontaine
School of Oceanography, University of Washington, Box 357940, Seattle, Washington 98115, USA (fontaine@ipgp.jussieu.fr)

Now at Equipe de Géosciences Marines, Institut de Physique du Globe de Paris, 4 Place Jussieu, Tour 24-14, F-75235 Paris, France

William S. D. Wilcock
School of Oceanography, University of Washington, Box 357940, Seattle, Washington 98115, USA

[1] Mid-ocean ridges host vigorous hydrothermal systems that remove large quantities of heat from the oceanic crust. Inferred Nusselt numbers (*Nu*), which are the ratios of the total heat flux to the heat flux that would be transported by conduction alone, range from 8 to several hundred. Such vigorous convection is not fully described by most numerical models of hydrothermal circulation. A major difficulty arises at high *Nu* from the numerical solution of the temperature equation. To avoid classical numerical artifacts such as nonphysical oscillatory behavior and artificial diffusion, we implement the Multidimensional Positive Definite Advection Transport Algorithm (MPDATA) technique, which solves the temperature equation using an iterated upwind corrected scheme. We first validate the method by comparing results for models with uniform fluid properties in closed- and open-top systems to existing solutions with $Nu \leq \sim 20$. We then incorporate realistic fluid properties and run models for *Nu* up to 50–60. Solutions are characterized by an unstable bottom thermal boundary layer where thermal instabilities arise locally. The pattern of heat extraction is periodic to chaotic. At any $Nu > \sim 13$ the venting temperatures in a given plume are chaotic and oscillate from ~350° to 450°C. Individual plumes can temporarily stop short of the surface for intervals ranging from tens to hundreds of years at times when other plumes vent with an increased flow rate. The solutions also display significant recirculation, and as a result large areas of downflow are relatively warm with temperatures commonly exceeding 150°C at middepths. Our results have important implications for mid-ocean ridge hydrothermal systems and suggest the following: (1) The reaction zones of mid-ocean ridge hydrothermal systems are enlarged by thermal instabilities that migrate laterally toward upflow zones. This will substantially increase the volume of rock involved in chemical reactions compared to steady state configurations. (2) Hydrothermal discharge can stop temporarily as zones of venting are dynamically replaced by zones of seawater recharge. (3) Anhydrite precipitation occurring at temperatures exceeding ~150°C will likely occur throughout a large portion of recharge zone and will not necessarily clog downflow pathways as efficiently as has been recently inferred.

Components: 10,028 words, 6 figures, 1 table.

Keywords: mid-ocean ridges; hydrothermal systems; modeling; high-Rayleigh; convection.

Index Terms: 0450 Biogeosciences: Hydrothermal systems (1034, 3017, 3616, 4832, 8135, 8424).

Received 4 February 2007; **Revised** 11 May 2007; **Accepted** 22 May 2007; **Published** 26 July 2007.

Fontaine, F. J., and W. S. D. Wilcock (2007), Two-dimensional numerical models of open-top hydrothermal convection at high Rayleigh and Nusselt numbers: Implications for mid-ocean ridge hydrothermal circulation, *Geochem. Geophys. Geosyst.*, *8*, Q07010, doi:10.1029/2007GC001601.

1. Introduction

[2] Mid-ocean ridges hydrothermal systems are the primary means for cooling newly formed ocean crust. Seawater sinks into the crust and is heated as it moves down toward the base of the system. Fluid-rock interactions alter the seawater composition and the hydrothermal solutions achieve chemical equilibrium at about 400°–450°C in a reaction zone [*Seyfried et al.*, 1991; *Seyfried and Ding*, 1995; *Butterfield et al.*, 2003] before rising quickly to the seafloor to vent in "smokers" at temperature up to 400°C. Areas of low-temperature and diffuse fluid emissions often surround smokers and result from the mixing of a high-temperature end-member fluid with cold seawater [*Butterfield et al.*, 2004; *Tivey et al.*, 1995] and the conductive heating of seawater in the shallow crust [*Cooper et al.*, 2000].

[3] The heat that drives convective circulation is mined from magma chambers at midcrustal depths (see *German and Lin* [2004] for a short review) or from a cracking front that penetrates hot rock [*Lister*, 1974, 1983; *Wilcock and Delaney*, 1996]. Heat flux estimates for large hydrothermal fields range from hundreds to thousands of MW [e.g., *Lowell and Germanovich*, 2004] with individual high-temperature vents (smokers) transporting between 1 and 10 MW [*Bemis et al.*, 1993; *Schultz et al.*, 1992, *MacDonald et al.*, 1980]. Inferred Nusselt numbers (*Nu*), which are the ratios of the total heat flux to the heat flux that would be transported by conduction alone, range from 8 [*Morgan and Chen*, 1993; *Henstock et al.*, 1993] to several hundreds [*Wilcock and Delaney*, 1996; *Lister*, 1983].

[4] Since their discovery in the mid-1970s [*Williams et al.*, 1974; *Corliss et al.*, 1979], these systems have been the focus of extensive modeling efforts. The physical processes are complex involving the vigorous flow of fluids with strongly nonlinear properties through a heterogeneous fractured porous medium whose permeability structure is poorly constrained and influenced by both physical and chemical feedbacks. In many systems, the flow is further complicated by sub- and/or super-critical phase separation of saline water and segregation of the resulting phases [*Lowell et al.*, 1995; *Lowell and Germanovich*, 2004, and references therein]. All models of the dynamics of these systems, inevitably involve simplifications [e.g., *Lowell*, 1991]. One general approach is to develop cellular convection models for flow through idealized permeability structures.

[5] Early studies focused on the interpretation of seafloor heat flow data [e.g., *Williams et al.*, 1974] using simplified, finite difference based, two-dimensional models. *Ribando et al.* [1976] carried out a series of numerical experiments using simple fluid properties (constant viscosity, linear density). Comparisons with data from the Galapagos spreading center [*Williams et al.*, 1974] led to a crustal permeability estimate of 4.5×10^{-16} m^2. *Fehn and Cathles* [1979] used pure water properties to model hydrothermal circulation across the axis of slow-spreading axis and advanced a model in which downflow occurs in wide areas while upflow concentrates in narrow zones (faults) of much higher permeability. *Fehn et al.* [1983] modeled the hydrothermal fields at the Galapagos spreading center and suggested that hydrothermal cells could move with the moving plate preventing the crust from reheating. *Rosenberg and Spera* [1990] and *Rosenberg et al.* [1993] used linear fluid properties to study the role of anisotropic and/or layered permeability in hydrothermal convection. *Travis et al.* [1991] developed the first three-dimensional models of mid-ocean ridge hydrothermal convection using linear fluid properties. More recently, *Wilcock* [1997] and *Cherkaoui et al.* [1997] used linear fluid properties to develop a model for event plumes and explain the decay of heat and venting temperature following a dike injection, respectively.

[6] About a decade ago, models started to incorporate more realistic, seawater-based fluid properties. *Rabinowicz et al.* [1998, 1999] used an equation of state for seawater (3.2 wt% NaCl) derived by *Potter and Brown* [1977] to compute single-phase, two- and three-dimensional models of circulation at sedimented and unsedimented

axes. Using the same equation of state, *Fontaine et al.* [2001] studied the effects of mineral precipitation/dissolution on the dynamics of mid-ocean ridge hydrothermal systems. *Wilcock* [1998] presented solutions obtained using an equation of state for seawater derived from *Pitzer et al.* [1984] and *Anderko and Pitzer* [1993], showing that the maximum venting temperature reaches ~65% of the bottom temperature instead of the 50% obtained when linear properties are used. Using this equation of state, *Cherkaoui et al.* [2003] modeled hydrothermal cooling at fast spreading ridges and *Fontaine and Wilcock* [2006] developed a model for the storage and dynamics of brines in mid-ocean ridges. *Schoofs and Hansen* [2000] employed temperature, pressure and salinity dependent fluid properties to describe the depletion of a brine layer at the base of mid-ocean ridge hydrothermal systems.

[7] Until quite recently limitations in computational capabilities and the lack of a well behaved equation of state for salt water restricted models to low Rayleigh numbers and single-phase flow. However, it is now possible to start develop models which overcome these limitations. Using linear fluid properties and the Boussinesq approximation, *Cherkaoui and Wilcock* [1999] present a series of two-dimensional numerical experiments of hydrothermal convection in open-top systems for Rayleigh numbers up to 1100 and show the development of periodic to chaotic circulation. *Xu and Lowell* [2000] study the dynamics of two-phase hydrothermal activity near a cooling dyke using pure water properties. *Kawada et al.* [2004] use an equation of state derived from *Anderko and Pitzer* [1993] to build a two-phase flow model at low Rayleigh numbers but their model does not include a full description of the segregation of the brine and vapor phases. *Geiger et al.* [2005] use finite element techniques and their own equation of state [*Geiger et al.*, 2006] to develop two-phase flow models of high permeability magmatic hydrothermal systems. Their work represents an important step in reducing the level of simplification in numerical models of mid-ocean ridge hydrothermal systems. Using the same numerical techniques but an equation of state for pure water at supercritical pressures, *Coumou et al.* [2006] model single phase hydrothermal activity for permeabilities up to 10^{-13} m^2. They show that hydrothermal circulation is unstable for permeabilities exceeding $\sim 10^{-15}$ m^2 with venting temperatures oscillating on timescales of tens to hundreds of years. They also describe the splitting of hot, buoyant rising plumes as they encounter cold, high viscosity downwelling fluids.

[8] A major difficulty in modeling thermal convection at high Rayleigh/Nusselt numbers arises from the numerical solution of the temperature equation. As the Rayleigh/Nusselt number increases, the characteristic time for advection keeps decreasing and may be considerably lower than the time for diffusion, leading to nonphysical oscillations near temperature fronts when classical centered finite difference methods are used [e.g., *Dubuffet et al.*, 2000]. Upwind schemes can be used to avoid these problems but such techniques introduce numerical diffusion that artificially stabilizes the flow [e.g., *Dubuffet et al.*, 2000]. Many techniques involving higher-order in space and time schemes have been developed to reduce these artifacts including the Total Variation Diminishing (TVD) [*Bell et al.*, 1986; *Durlofsky et al.*, 1992; *Geiger et al.*, 2004, 2006, and reference therein], the Flux-Corrected Transport (FCT) [*Zalesak*, 1979], the Essentially Non-Oscillatory (ENO) [*Harten et al.*, 1987] and the Multidimensional Positive Definite Advection Transport (MPDATA) [*Smolarkiewicz*, 1984] numerical algorithms. In this paper, we describe the application of the MPDATA technique to avoid these numerical artifacts. We first benchmark the technique using uniform fluid properties. We then present two-dimensional, single-phase models of hydrothermal convection with realistic, seawater-based fluid properties for Rayleigh numbers, Nusselt numbers and permeabilities up to 5000, 60, and 10^{-14} m^2, respectively. Our results reproduce features observed by *Coumou et al.* [2006] such as the unstable flow and venting temperature fluctuations. They also have important implications for the thermal structure of the downflow zone and for the volume of rock in the reaction zone.

2. Modeling High-*Nu* Hydrothermal Circulation

[9] We adopt a porous flow model to describe the single-phase flow driven by a vertical temperature difference of ΔT across a two-dimensional vertical domain of dimensions $H \times H$ (Figure 1). The base of the system is impermeable and isothermal. For the purpose of benchmarking, we consider systems with open and closed tops but only open-top systems are considered when modeling mid-ocean ridges. In open-top systems, the top interface is at a constant pressure which results in vertical flow at the interface with the fluid being free to enter at a

constant temperature (2°C for mid-ocean ridge models) and leave the system with a zero cooling rate ($\partial T/\partial z = 0$). In close-top systems, the upper interface is impermeable and no flow crosses the interface. The vertical sides of the system are impermeable and are planes of symmetry for the temperature and flow fields which results in no fluid or heat flow across the boundary.

2.1. Continuity and Flow Equations

[10] Neglecting transient density variations the continuity equation is

$$\frac{\partial(\rho u)}{\partial x} + \frac{\partial(\rho v)}{\partial z} = 0 \tag{1}$$

and we assume the flow obeys Darcy's law

$$u = -\frac{k}{\mu}\frac{\partial p}{\partial x} \tag{2}$$

$$w = -\frac{k}{\mu}\left(\frac{\partial p}{\partial z} - \rho g\right) \tag{3}$$

Here x and z (positive downward) designate the Cartesian coordinates, u and w are the horizontal and vertical components of the Darcy velocity, p is the fluid pressure, g is the gravitational acceleration, ρ and μ are the fluid density and viscosity, respectively, and k is the permeability of the system.

[11] We define the stream function ψ

$$\frac{\partial \Psi}{\partial z} = \rho u \tag{4a}$$

$$\frac{\partial \Psi}{\partial x} = -\rho w \tag{4b}$$

Eliminating pressure by taking the curl of equations (1) and (2) leads to

$$\frac{1}{R}\nabla^2\Psi = -\left(\frac{\partial}{\partial x}\left(\frac{1}{R}\right)\frac{\partial \Psi}{\partial x} + \frac{\partial}{\partial z}\left(\frac{1}{R}\right)\frac{\partial \Psi}{\partial z}\right) - \frac{\partial\left(\rho_f\right)}{\partial x} \tag{5}$$

where R is the hydraulic conductivity $R = k\rho g/\mu$.

[12] The problem is nondimensionalized by scaling lengths with H, time with H^2/κ, temperature with ΔT, and velocities with κ/H where κ is the thermal diffusivity of the porous medium. The dimensionless form of equation (5) depends on the nature of the fluid thermodynamic properties. In section 3 we benchmark our models with solutions from previous studies where simple uniform properties were used. Here, the viscosity $\mu = \mu_c$ is constant and the density ρ decreases linearly with temperature following $\rho = \rho_o(1 - \alpha(T - T_o))$, where ρ_o, and T_o are the reference density and temperature, respectively and α is the thermal expansivity. The dimensionless form of equation (5) is then

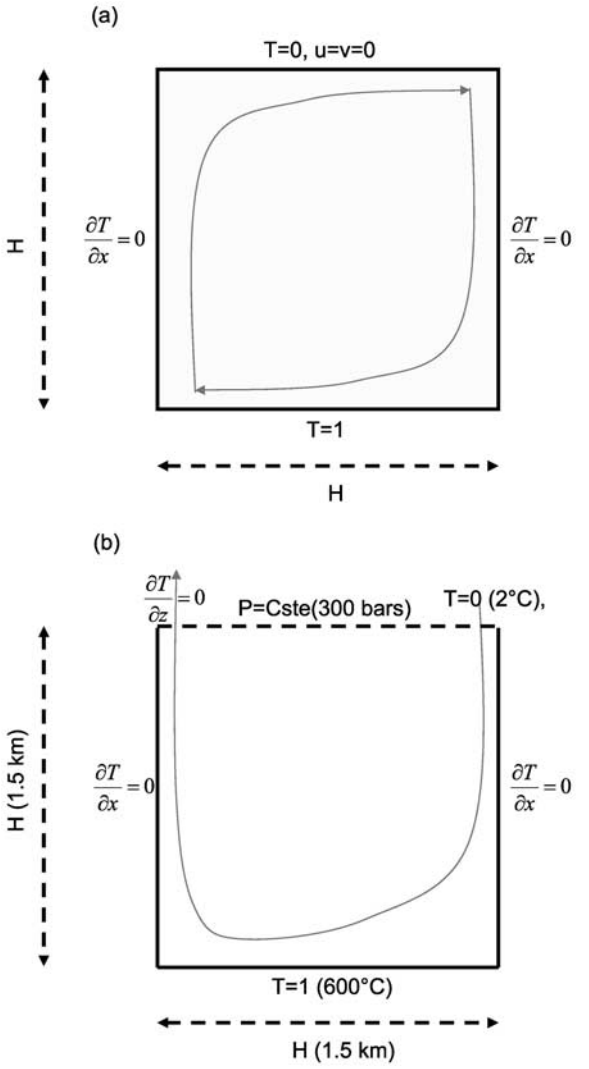

Figure 1. Model setup for (a) closed- and (b) open-top systems.

$$\nabla^2\Psi = Ra^l\frac{\partial \theta}{\partial x} \tag{6}$$

where θ is the dimensionless temperature ($\theta = T/\Delta T$) and Ra^l is the Rayleigh number (superscript l refers to the linear fluid properties) which accounts for

the vigor of the convective circulation and is given by

$$Ra^{l} = \frac{\rho_o g H \alpha \Delta T k}{\mu_c \kappa} \tag{7}$$

[13] In addition to the Rayleigh number we define the Nusselt number *Nu* which provides a dimensionless measure of the heat flux across the porous medium. For a layer heated from below we write

$$Nu = -\int_0^1 \left.\frac{\partial \theta}{\partial z}\right|_{z=0} dx \tag{8}$$

[14] In section 4 we apply our models to mid-ocean ridge hydrothermal circulation and use temperature and pressure dependent density and viscosity. The density is obtained using the equation of state of *Pitzer et al.* [1984] at temperatures $\leq$300°C and *Anderko and Pitzer* [1993] at temperature >300°C. The viscosity of the hydrothermal fluid is derived using the relationship of *Meyer et al.* [1993]. At the high temperatures (>400°C) and pressures (>300 bars) typical of mid-ocean ridges hydrothermal systems, seawater-based fluid can phase separate into a high-salinity brine and low-salinity vapor and the flow becomes two-phase. Modeling two-phase flow relevant to mid-ocean ridges currently represents a major challenge mostly because the equation of state for the H_2O-NaCl and the segregation process (i.e., the way the brines and vapors physically separate) are poorly known. Although some recent studies have started to investigate the characteristics of hydrothermal circulation with models that include the phase separation of seawater and the segregation of the resulting two phases [*Geiger et al.*, 2005; *Kissling*, 2005], their output still needs to be compared to results from other codes.

[15] The development of such two-phase flow models is out of the scope of this paper. In the two-phase area we follow the approach adopted by *Wilcock* [1998] and assume weighted mean properties of the brine and vapor phases. This approach is presumably accurate at least when a relatively small amount of brine is present in the system and should provide a reasonable approximation to flow in a system which is mostly single-phase except in a thin, super-critical reaction zone at its base. Vapor-dominated transport in mid-ocean ridge systems is probably a reasonable assumption as stated by *Geiger et al.* [2005]. The dimensionless form of equation (5) is then

$$\frac{1}{r}\nabla^2 \psi = -\left(\frac{\partial}{\partial x}\left(\frac{1}{r}\right)\frac{\partial \Psi}{\partial x} + \frac{\partial}{\partial z}\left(\frac{1}{r}\right)\frac{\partial \Psi}{\partial z}\right) + Ra^{nl}\left(\frac{\partial(\chi(\theta,\Pi))}{\partial x}\right) \tag{9a}$$

$$Ra^{nl} = \frac{\Delta\rho g H k}{\mu_o \kappa} \tag{9b}$$

$$\chi(\theta,\Pi) = -\left(\frac{\rho(T,P)-\rho_o}{\Delta\rho}\right) \tag{9c}$$

[16] Ra^{nl} is the Rayleigh number (superscript *nl* refers to the nonlinear fluid properties), $\Delta\rho$ is the density contrast between hot and cold fluid, and μ_o and ρ_o are the viscosity and density at the bottom of the system, respectively. When the bottom temperature is 600°C$\Delta\rho$ = 910 kg/m^3; $\mu_o = 5 \times 10^{-5}$ Pas and ρ_o = 130 kg/m^3. The term r = R/R$_o$ (R$_o$ = kg/μ_o) is the dimensionless resistivity and χ is a dimensionless function that scales the density variations. Π is the dimensionless pressure and satisfies

$$\Pi = \frac{k_o}{\mu_o \kappa}(p - \rho_o g z) \tag{10}$$

[17] The stream function is discretized on a $n \times n$ points, staggered grid and solved using the following spectral decompositions

open top

$$\Psi(x,z) = \sum_{i=1,n}\sum_{j=1,l} \Psi_{i,j} \sin(i\pi x)\cos\left((2j+1)\tfrac{\pi z}{2}\right) \tag{11a}$$

close top

$$\Psi(x,z) = \sum_{i=1,n}\sum_{j=1,l} \Psi_{i,j} \sin(i\pi x)\sin(j\pi z) \tag{11b}$$

[18] These decompositions are valid for a two-dimensional flow in a box with impermeable vertical boundaries but with an open (equation (11a)) and closed top (equation (11b)) [*Rabinowicz et al.*, 1999; *Fontaine et al.*, 2001].

2.2. Temperature Equation

[19] Under the assumption that the fluid and the rock are in thermal equilibrium, the equation governing

Table 1. Comparisons of Solutions for Various Numerical Experiments in Closed- and Open-Top Systems

	Closed-Top			Open-Top			Source
Ra	800	950	1200	550	1000	1075	
Nu[a]	9.2	10.9	13.06	12.14	18.2	20.1	this study
f1	275	397	608		490	477	
f2		200	228			95	
Nu	9.14			12.1[b]	18.35[b]	20.3[b]	*Cherkaoui and Wilcock* [1999]
f1	299.7				514 ± 5	522 ± 4	
f2						84 ± 2	
Nu	9.0[b]	11[b]					*Graham and Steen* [1994]
f1	285[b]	404 ± 2	640				
f2		176 ± 2	232				
Nu	9.3[b]	11.2[b]					*Kimura et al.* [1986]
f1	280[b]	422[b]					
f2		164[b]					

[a] When the circulation is unsteady, Nusselt numbers are taken as mean over a typical timescale.
[b] Values read from graphs in the article.

heat transfer in the porous medium is

$$(\rho c)_{eq}\frac{\partial T}{\partial t} + (\rho c)_f \nabla.(\vec{v}T) = \lambda_{eq}\nabla^2 T \qquad (12a)$$

$$\Leftrightarrow \frac{\partial T}{\partial t} + \nabla.(\vec{v}T) = \kappa\nabla^2 T \qquad (12b)$$

where t is time, $(\rho c)_{eq}$ and $\lambda_{eq} = 2.5$ W/m°K are the volumetric heat capacities and thermal conductivity of the fluid saturated porous medium, respectively, $(\rho c)_f = 4.2 \times 10^6$ J/Km^3 is the volumetric heat capacities of the fluid, T is the temperature and $\vec{v}(u, w)$ is the velocity vector. Considering that the ratio $\gamma = (\rho c)_f/(\rho c)_{eq}$ is close to unity, the thermal diffusivity of the fluid saturated porous medium is $\kappa = (\lambda)_{eq}/(\rho c)_f = 6 \times 10^{-7}$ m^2/s.In its dimensionless form the temperature (θ) equation is

$$\frac{\partial \theta}{\partial t} + \vec{\nabla}.(\vec{v}\theta) = \vec{\nabla}^2\theta \qquad (13)$$

[20] The temperature equation is discretized on the $n \times n$ points, staggered grid and solved with the Multidimensional Positive Definite Advection Transport Algorithm (MPDATA) devised by *Smolarkiewicz* [1984]. MPDATA is a finite difference, second-order accurate, explicit scheme for approximating the advective terms in fluid equations. The temperature equation (equation (13)) is an advection-diffusion equation but can be written as an advection equation following [*Smolarkiewicz and Clark*, 1986]

$$\frac{\partial \theta}{\partial t} + \vec{\nabla}.\left[(\vec{v} - \vec{v}_{diff})\theta\right] = 0 \qquad (14a)$$

$$\vec{v}_{diff} = \frac{1}{\theta}\vec{\nabla}\theta \qquad (14b)$$

The first pass of the MPDATA scheme is a simple upwind approximation that is first-order accurate. The upwind scheme introduces a coefficient of artificial diffusion that is proportional to the grid Peclet number Pe_g^i (i = x, z, $Pe_g^x = (u - u_{diff})/dx$, $Pe_g^z = (w - w_{diff})/dz$) [*Dubuffet et al.*, 2000]. The amplitude of the artificial diffusion increases with the vigor of the convective flow and reduces its intensity which can eventually stabilize flows that are inherently unsteady. To avoid this issue, the MPDATA scheme uses a second pass to estimates and compensates for the artificial error of the first pass. Additional passes can be used to increase further the accuracy of the solution.

3. Test Case: Convection in Open and Closed Boxes

[21] A number of authors have studied the characteristics of convection in a porous boxes heated

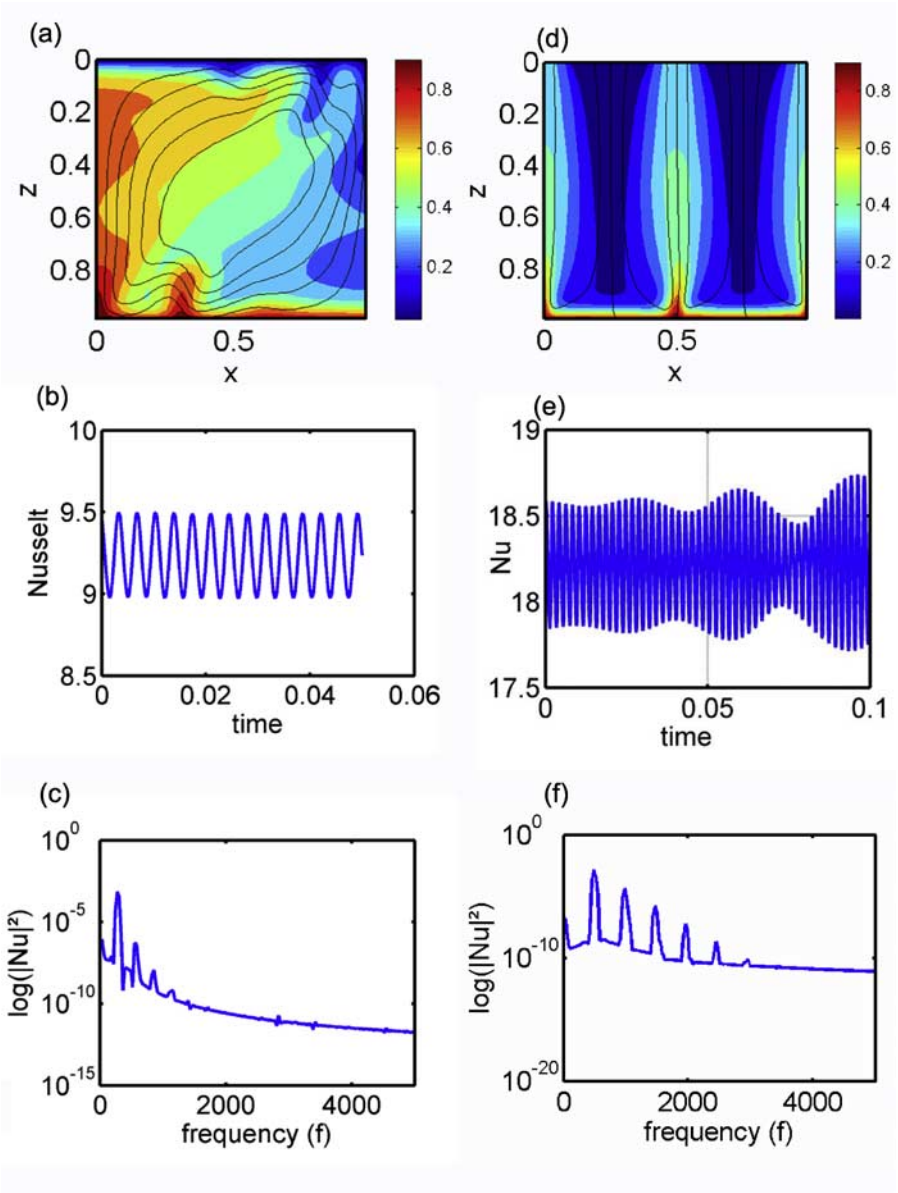

Figure 2. (a–c) Unsteady convection in a closed-top system at Ra = 800. (a) Dimensionless temperature field (shading) and stream function (black lines). (b) Nusselt number as a function of time. (c) Power spectrum of the Nusselt number. One fundamental frequency f = 275 prevails at Ra = 800. (d–f) Same as Figures 2a–2c but for an open-top system at Ra = 1000. One fundamental frequency f = 490 prevails at Ra = 1000.

from below in closed-top [e.g., *Kimura et al.*, 1986; *Steen and Aidun*, 1988; *Caltagirone and Fabrie*, 1989; *Graham and Steen*, 1994; *Cherkaoui and Wilcock*, 1999] and open-top systems [*Cherkaoui and Wilcock*, 1999]. In these studies, the fluid has uniform thermodynamic properties (i.e., constant viscosity and expansivity), the density decreases linearly with temperature, and the Boussinesq approximation is used. In order to benchmark our numerical model, we obtained solutions to equations (6) and (14) for various Ra^l and compared them to results from previous studies for both the open and closed-top conditions. Close-top and open-top solutions were obtained on grids composed of 64 × 64 and 128 × 128 points, respectively.

[22] Our solutions yield Nusselt numbers and frequencies of oscillation, f, that compare reasonably well with those of *Kimura et al.* [1986], *Graham and Steen* [1994], and *Cherkaoui and Wilcock* [1999] (Table 1). For the closed-top systems, our numerical solution at Ra^l = 800 (Figures 2a–2c) is single-periodic and the mean Nu and frequency

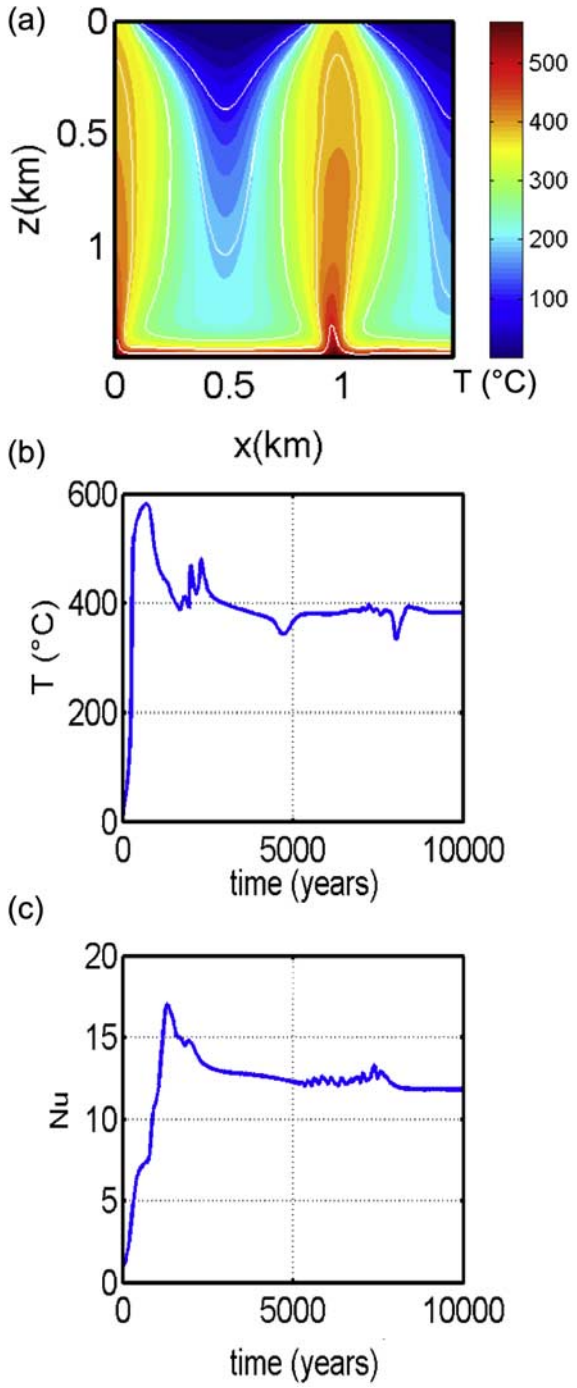

Figure 3. Characteristics of hydrothermal convection in a system with realistic fluid properties for a permeability $k = 2.25 \times 10^{-15}$ m^2 ($Ra = 1000$). The temperature at the base of the system is set to 600°C. (a) Two-dimensional temperature field overprinted with white lines representing the 100°, 200°, 300°, 400°, and 500°C isotherms. (b) Venting temperature at the axis of the upflow zone located on the left side of the system. (c) Nusselt number as a function of time. The circulation is composed of two upflow and two downflow zones and reaches steady state. Maximum venting temperatures are about 380°C.

number are in reasonable agreement with previous studies (Table 1). At $Ra^l = 1200$ we find a chaotic regime with two oscillation frequencies which closely match those reported by *Graham and Steen* [1994]. For open-top systems, when $Ra^l = 550$, the circulation is steady and $Nu = 12.15$ (Table 1). When $Ra^l = 1000$, the circulation is unsteady and single-periodic with a mean Nu and frequency close to the one obtained by *Cherkaoui and Wilcock* [1999] (Figures 2d–2f).

4. Modeling Mid-Ocean Ridge Hydrothermal Systems

[23] In order to simulate mid-ocean ridge hydrothermal circulation we incorporated realistic fluid properties into the models and solved equations (9a) and (14) in a square box measuring 1.5 km × 1.5 km. Solutions were obtained on grids with sizes ranging from 128 × 128 to 384 × 384. The pressure at the top of the domain is 300 bars and the basal temperature is set to 600°C. Although the temperature of axial hydrothermal fluids may reach 700°–750°C [*Gillis et al.*, 2001; *Manning et al.*, 1996] at the brittle-ductile transition zone [*Hirth et al.*, 1998], flow at the highest temperatures may not contribute significantly to large scale circulation as the permeability and density of throughgoing fissures likely decrease as temperatures approach the brittle-ductile transition [*Nehlig*, 1994]. In Figure 3 we show the result of an experiment on a grid composed of 192 × 192 points for a Rayleigh number Ra^{nl}(equation (9b)) of 1000 which corresponds to a permeability of $k = 2 \times 10^{-15}$ m^2. The circulation is composed of two upflow and downflow areas (Figure 3a) and reaches steady state with a maximum venting temperature of ~380°C (Figure 3b) and a Nusselt number of 13 (Figure 3c). We obtained similar solutions on grids with dimensions ranging from 128 × 128 to 384 × 384. We used this steady state solution as the initial condition for experiments with higher Rayleigh numbers.

[24] Figure 4 shows a solution for $Ra^{nl} = 2000$ ($k = 4 \times 10^{-15}$ m^2) obtained with a 256 × 256 grid. Similar solutions were also obtained on a 128 × 128 grid. The circulation is composed of three upwelling plumes and two regions of downflow areas (Figure 4a). The base of the system is unstable and thermal instabilities arise in the bottom thermal boundary layer. These instabilities move horizontally and are collected by robust upwelling plumes. As a consequence, the Nusselt fluctuates from ~19 to ~27 (Figure 4c). The power

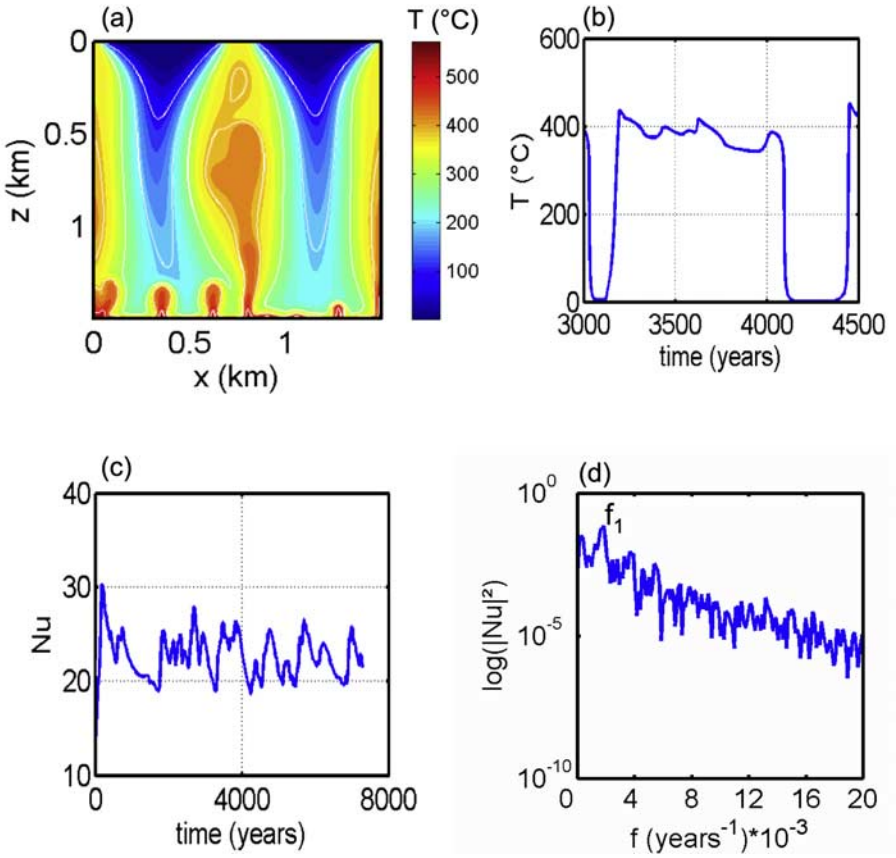

Figure 4. (a–c) Same as Figure 3 but for a permeability of $k = 4.5 \times 10^{-15}$ m^2 ($Ra = 2000$). The circulation is composed of three major zones of upwelling that collect the thermal instabilities that form in the thermal boundary layer at the base of the system. The circulation is unsteady, and maximum venting temperatures vary from ~350°C to ~450°C. Note the sharp drops in temperature when individual upflow zones are temporarily capped by regions of downflow. These events have typical timescales of a few hundred years. (d) Power spectrum of the Nusselt number. The Nusselt number fluctuates on timescales of ~650 years.

spectrum of this Nusselt number (Figure 4d) shows that the circulation has a strong single periodic component with a peak at a frequency of $\sim 1.5 \times 10^{-3}$ years^{-1} which corresponds to a periodicity of ~650 years.

[25] Although the spatial distribution of upflow versus downflow remains stable, individual plumes often temporarily stop short of the surface, a phenomenon that was also observed by *Coumou et al.* [2006]. This pattern is linked to the advection of instabilities across the seafloor. When a plume collects an instability it strengthens and upflow velocities increase in the vicinity of the instability. When the instability reaches the surface the outflow velocities increase and in order to maintain the balance of inflow and outflow fluxes, the outflow velocities in adjacent plumes must decrease. In many instances outflow in individual plumes stops altogether and is replaced by the inflow of cold seawater for intervals of up to several hundred years. Eventually, the influx of hot fluid into the stalled plume makes it sufficiently buoyant to rise through the cold seawater layer and high temperature venting resumes. This may or may not result in the cessation of venting in another plume. This process is illustrated in Figure 5a, which shows the heat flux across the seafloor as a function of horizontal position. The maximum heat flux at any given time ranges from ~50 W/m^2 to >300 W/m^2. Plumes tend to stall when or shortly before the heat flux exceeds 200 W/m^2 in another plume.

[26] Venting temperature also oscillates and their maximum ranges from ~350° to ~450°C (Figure 4b). The arrival of instabilities at the surface leads to a spike in the venting temperature (Figure 4b). However, the timescale of the temperature oscillations are not directly link to the time-

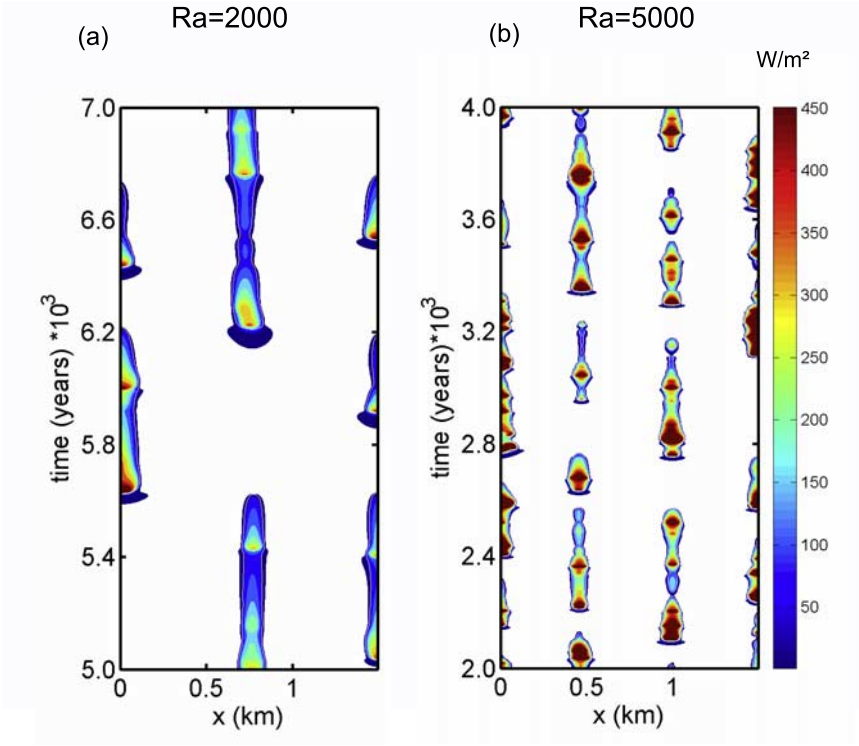

Figure 5. (a) Temporal variations of the heat flux (W/m^2) at different locations on the seafloor for the model of Figure 4, which has a permeability of $k = 4.10^{-15}$ m^2 ($Ra = 2000$). The shaded areas correspond to the heat flux of each individual venting sites; the white areas correspond to zones of downflow. Overprinted white lines represent the 300°C isotherm. A large part of the fluid vents at temperatures >300°C. Corresponding heat flux ranges from ~50 W/m^2 to 200 W/m^2. Note that when the plume located on the left side stops short of the surface, the heat flux of the "middle" plume increases. (b) Same as Figure 5a but for the model of Figure 6, which has a permeability of 10^{-14} m^2 (Ra = 5000). The heat flux ranges from 100 W/m^2 to >400 W/m^2.

scale of Nusselt number oscillations and the temperature oscillations show no clear single periodicity. This is partly because the thermal instabilities that form in the bottom boundary layer loose their higher frequency structure as a result of diffusion as they move through the upflow zone. More importantly, the temperatures in a given plume are only affected by the instabilities that are advected into it, and it appears that instabilities are apportioned between plumes in an unpredictable manner. This chaotic collecting process coupled with variable rates of upward advection in the plumes, acts to decorrelate the variations of the venting temperature in a particular plume from the oscillations of the Nusselt number. Auxiliary material Movie S1[1] illustrates the dynamical behavior (e.g., unstable thermal boundary layer, capping of upwellings) of a system in which $Ra = 2000$ (k = 4.10^{-15} m^2) over a period of ~1000 years.

[1]Auxiliary materials are available in the HTML. doi:10.1029/2007GC001601.

[27] Figure 6 shows solutions for $Ra^{nl} = 5000$ (k = 10^{-14} m^2) obtained on a grid with 384 × 384 points; solutions with similar characteristics are obtained for a 256 × 256 grid. The circulation is composed of four upwelling and three downwelling regions (Figure 6a) and the Nusselt oscillates between ~45 and ~60 (Figure 6c). We note that the increase in the number of plumes as the Rayleigh increases from 1000 to 5000 is consistent with a simple scale analysis which shows that the number of plumes should scale as $(Ra^{nl})^{1/2}$ [*Lowell and Germanovich*, 2004].

[28] When $Ra^{nl} = 5000$, the power spectrum is much noisier than for $Ra^{nl} = 2000$, but there is a broad region of high energy for frequencies ranging from ~3 × 10^{-3} to ~6 × 10^{-3} years^{-1} with several peaks inside (Figure 6d) which is indicative of a chaotic behavior [*Graham and Steen*, 1994]. The maximum venting temperature oscillates between ~380° and ~450°C (Figure 6b). The solutions still show intervals when venting ceases

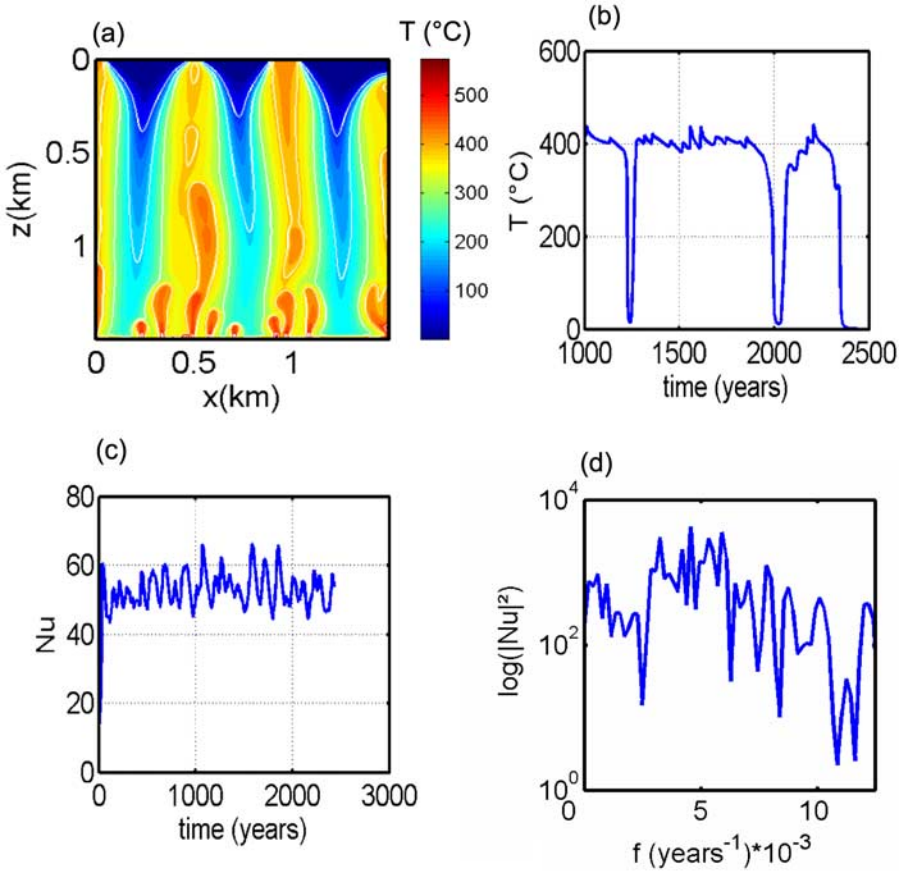

Figure 6. Same as Figure 4 but for a permeability of $k = 1.12 \times 10^{-14}$ m^2 ($Ra = 5000$). The circulation is composed of four major zones of upwelling. Maximum venting temperatures vary from ~380°C to 450°C. The sharp drops in venting temperature that delineate intervals when ouflow ceases have typical timescales of tens to one hundred years. The circulation is unsteady, and the Nusselt number displays weakly chaotic behavior.

at particular sites but on the timescales of only a few tens of years (Figures 6b and 5b). The maximum venting heat flux at a given time ranges from 100–150 W/m^2 to 400–450 W/m^2 (Figure 5b).

5. Discussion

[29] Mid-ocean ridge hydrothermal systems remove large quantities of heat from the oceanic crust. The Nusselt number Nu which is defined in equation (8) can be written equivalently as

$$Nu = \frac{QH}{\lambda \Delta T} \tag{15}$$

where ΔT(°C) is the temperature contrast in the system, $\lambda = 2.5$ W/m°C is the thermal conductivity of the fluid-filled crust, Q(W/m^2) is the average heat flux per unit area and H(m) is the depth of circulation. Quantifying the heat flux of a given system is difficult because it requires an estimate of the power of the vent field and of the horizontal dimensions of circulation cell. Power estimates for individual hydrothermal fields range from hundreds to thousands of MW [e.g., *Lowell and Germanovich*, 2004]. Accurate measurements over the Main Field vent sites on the Endeavour segment of the Juan de Fuca Ridge indicates a heat flux of 600 ± 50 MW and the ratio of the heat fluxes from focused and diffuse sources is estimated to be one [*Veirs et al.*, 2006]. Estimates for the heat uptake area are typically 10^5 to 10^6 m^2 [e.g., *Lowell and Germanovich*, 2004]. At the Main Endeavour Field, *Wilcock and Fisher* [2004] estimate a heat uptake area of 2 km^2. Dividing the vent field power estimates by the estimates of the heat uptake area, and considering that the systems with the highest powers are likely to have the highest heat uptake area, yields typical values for Q ranging from a few tens to a few hundreds of W/m^2.

[30] The depth of circulation H varies depending on the hydrothermal setting. Hydrothermal fluids circulate in the axis of mid-ocean ridges through a network of fissures and fractures that result from the brittle fracturing of the crust under tensional stress. The depth of fracturing/penetration is controlled by the brittle-ductile transition which likely occurs at a temperature of 700°–750°C [*Hirth et al.*, 1998]. At fast and medium spreading ridges and at least at one location on slow-spreading axes, the Lucky Strike volcano on the Mid-Atlantic Ridge [*Singh et al.*, 2006], seismic reflection studies image a sill-like, partially of fully molten, magma chamber 1–3 km below the seafloor [see also *German and Lin*, 2004, and references therein]. The brittle-ductile transition occurs at these depths, in the thin gabbroic section a few meters to hundreds of meters thick [*Toomey et al.*, 1994; *Singh et al.*, 1999; *Lowell and Germanovich*, 2004] between the base of the dikes and the melt lens.

[31] Equating ΔT to the difference between the temperature at the brittle-ductile transition ($T \approx 750$°C [e.g., *Hirth et al.*, 1998]) and the temperature of cold seawater (2°C), equation (15) yields Nu ranging from a few tens to a few hundreds. In this paper we have studied the characteristics of hydrothermal convection for Nu up to 60 ($k = 10^{-14}$ m^2), and have been able to check the consistency of our solutions at two different grid resolutions. Models with significantly higher Nusselt number (or permeability) would require a denser computing grid and their numerical cost is beyond the scope of this study.

[32] *Coumou et al.* [2006] succeed in running experiments for hydrothermal convection in a medium with permeabilities up to 10^{-13} m^2 but used properties for pure water at supercritical temperatures. It is difficult to determine whether their ability to obtain these high-permeability solutions reflects the differences in numerical techniques and available computational power or the different fluid properties. At supercritical pressures the properties of pure water vary more smoothly with temperature and pressure than those of seawater.

[33] Our models show that for permeabilities $k > 2 \times 10^{-15}$ m^2 ($Nu > \sim 13$) the pattern of heat extraction by hydrothermal circulation displays unsteady behavior. When $k = 4 \times 10^{-15}$ m^2 ($Nu = 19 - 27$), we find a periodic solution with a typical periodicity of ~600 years while at $k \geq 10^{-14}$ m^2 ($Nu = 45 - 60$), the circulation is chaotic. Maximum venting temperatures range from 380°C and up to 450°C. In some ways these results are similar to previous numerical experiments for open-top systems using both constant fluid properties [*Cherkaoui and Wilcock*, 1999] and pure water fluid properties [*Coumou et al.*, 2006]. These studies also see an evolution from steady to periodic to chaotic flow as the Rayleigh number increases. *Coumou et al.* [2006] found that there is a threshold permeability $k = \sim 10^{-15}$ m^2 above which the circulation is unsteady, a value that is in good agreement with our results. Our asymptotic maximum venting temperature of ~380°C is also in good agreement with theirs for this permeability.

[34] For higher permeabilities at which the circulation is unsteady, our results differ from *Coumou et al.* [2006] in a few ways. If we compare solutions for $k = 10^{-14}$ m^2 (compare our Figure 6 with Figure 2 of *Coumou et al.* [2006]), our venting temperatures are higher and fluctuate between 380° and 450°C, while those of *Coumou et al.* [2006] range from 380° to ~400°C. One reason for this difference is the different model setup. *Coumou et al.* [2006] obtained solutions for hydrothermal circulation for different pressure (250–350 bars compared with 300–450 bars) and temperature (2°–1000°C compared with 2°–600°C). They used pure water properties as opposed to the seawater-based properties used here, and considered systems with a larger aspect ratio (width divided by height). The higher venting temperature in our solutions may result from the higher pressure range since maximum upwelling temperatures increase with pressure [*Jupp and Schultz*, 2000].

[35] Another possible reason is that *Coumou et al.* [2006] use pure water rather than seawater properties. *Coumou et al.* [2006] note that their venting temperatures are in good agreement with the fluxibility theory developed by *Jupp and Schultz* [2000]. On the basis of a determination of the temperature at which plumes transport heat most efficiently, *Jupp and Schultz* [2000] argue that for basal temperature >500°C, plumes of pure water form naturally at a temperature of ~400°C and that the venting temperature cannot be higher than this value. However, they recognize that for seawater this maximum temperature should increase by about 30°C. The work of *Geiger et al.* [2005] supports this hypothesis and shows that for basal pressures between 400 and 500 bars, maximum venting temperatures could range between 420° and >500°C which is consistent with the range of temperature we observe.

[36] While we can reconcile our maximum venting temperatures of ~450°C with other studies, it is

important to note that temperatures this high have never been observed in real systems. One explanation for this discrepancy is that the layered permeability structure of oceanic crust in which high-permeability pillows overly lower permeability sheeted dikes results in a significant decrease in venting temperatures. Several previous studies have concluded that the hot fluid cools significantly as it passes through the high-permeability pillows both by conduction and by mixing with the seawater circulating in shallow secondary cells [*Pascoe and Cann*, 1995; *Wilcock*, 1998; *Fontaine and Wilcock*, 2006]. An alternative explanation is that the effective basal temperatures in real systems are not as high as the 600°C used for our solutions, and that real systems thus do not quite achieve the temperatures predicted by the fluxibility argument. For example if phase separation leads to the building of a brine layer at the base of the system preventing seawater from reaching the deepest parts of the system [e.g., *Bischoff and Rosenbauer*, 1989; *Fontaine and Wilcock*, 2006], the actual bottom temperature for the seawater-dominated cells would be lower.

[37] At k = 10^{-14} m^2, our population of instabilities in the bottom boundary layer is much denser than that of *Coumou et al.* [2006]. This may likely be a result of the differences between the equations of state and in the assumed height and pressure range for the models as discussed above. In particular, our models consider that the ratio γ of the fluid volumetric heat capacity (ρc_f) by the rock volumetric heat capacity is close to unity over the temperature and pressure domain, an assumption that is reasonably accurate at temperatures lower than ~450°C which prevail everywhere except in a thin basal thermal boundary layer which is a few tens of meters thick. Here temperatures increase sharply with depth from 450°C to 600°C and γ drops by about one order of magnitude. Since the ratio γ appears in the advective part of the temperature equation, our models will overestimate the efficiency of the advective processes at the base of the system which may partly account for the fact that our bottom boundary layer is more buoyant than the one of *Coumou et al.* [2006]. We also note that for this experiment our grid size (~4 × 4 m^2) is smaller than the one used in the experiment of *Coumou et al.* [2006] (i.e., 7 × 10 m^2). Consequently, the bottom boundary layer is likely better resolved in our experiment and this may also lead to differences in the oscillating behavior of the system.

[38] Our models also neglect the transient density variations in the mass conservation equation (equation (1)). A two-phase vapor/brine mixture at high temperature is compressible [*Geiger et al.*, 2006] and transient density variation should ideally be taken into account. By not including this term we are able to use the stream function with a spectral decomposition technique that is known to yield a more accurate solution for the flow at boundary layers [e.g., *Fornberg*, 1998]. The solution of a transient parabolic, pressure-diffusion equation with dedicated finite difference or finite volume method would allow the inclusion of transient density variations, but for a given grid resolution would lead to a less accurate solution for flow at the bottom boundary layer. It is unclear if the higher accuracy achievable in the boundary layer with our technique outweighs the loss of accuracy due to the exclusion of transient density terms, although we note that high resolution in the bottom boundary layer is particularly important for chaotic flow at high Rayleigh/Nusselt numbers.

[39] In real systems, the high concentrations of "soluble" elements such as Li, Rb, Cs and B in the venting fluids [e.g., *Von Damm*, 1995] require an abundance of fresh basaltic rock relative to the mass of seawater [*Seyfried and Ding*, 1995]. The fact that time series analysis of fluid composition have failed to reveal any significant differences in the flux of these elements on periods of order a decade or more [*Butterfield and Massoth*, 1994; *Von Damm*, 2004; *Von Damm et al.*, 2005] have been interpreted in terms of continuous penetration of hydrothermal fluids into unaltered/fresh rocks in the reaction zone at the base of the system [*Seyfried and Ding*, 1995]. Our results indicate that for permeabilities >10^{-15} m^2, the reaction zone of mid-ocean ridges are unsteady and that small thermal instabilities arise and move laterally to be collected by strong plumes. This provides a means for a hydrothermal system to react at high temperatures with a much larger volume of rock at any given time than if the reaction zone were limited to a thin steady state thermal boundary layer [e.g., *Lowell and Germanovich*, 2004] and thus may lead to fluids compositions that are stable over longer periods. When *Ra* = 2000 and k = 4.10^{-15} m^2, the lifetime of the small thermal instabilities is of the order 50–100 years (Movie S1[1]). This lifetime will decrease roughly linearly with the permeability and will range from a few years to a few tens of years for more realistic permeabilities of 10^{-14}–10^{-13} m^2. In this model, the boundaries of the reaction zone also change

with time as the instabilities migrate laterally. By this mechanism, fluid composition might remain stable without having to invoke the mining of fresh rock by downward penetration of the hydrothermal system.

[40] An interesting phenomenon observed in our solutions and by *Coumou et al.* [2006] is the temporary cessation of venting in individual plumes that occurs when others vent at higher velocities. These periods of quiescence have typical timescales that decrease as *Nu* increases and last from tens to hundreds of years. The TAG hydrothermal field is a 5 × 5 km^2 area located in the axial valley at 26°08′N on the Mid-Atlantic Ridge. At least five ∼200 m-wide, sulfide mounds, of which only the southern one is currently active and emitting black and white smoker fluids at temperature up to 365°C, lie along a series of axis-parallel faults [*Rona et al.*, 1993; *White et al.*, 1998]. Detailed dating of hydrothermal precipitates reveals a complex history made of episodes of venting followed by periods of rest [*Lalou et al.*, 1995]. Many of the sulfide mounds in the area have vented at the same time in the past while other were inactive. During these periods of quiescence, mounds cool and aragonite forms as seawater flows in [*Lalou et al.*, 1995]. Classically, this episodicity has been attributed to episodic volcanic eruptions in the area [*Zonenshain et al.*, 1989; *Humphris and Cann*, 2000] or to the interplay between mineral clogging and seismic activity [*White et al.*, 1998]. On the basis of our experiments, we suggest that the episodic nature of hydrothermal venting at TAG and its migration between different sites might be explained at least in part by the characteristics of the flow in a system heated steadily from below. However, our inferences do not take into account the dynamical coupling between magmatic (e.g., convection, freezing and replenishment) and hydrothermal processes which are also likely to control the natural variability of heat output and vent temperature.

[41] Our models also have interesting implications for the temperature distribution in the crust and the patterns of mineral precipitation. The solutions display significant recirculation and areas of downflow are relatively warm with temperature commonly exceeding 150°C at middepths (Figure 6a). This temperature distribution contrasts with models with uniform fluid properties [e.g., *Cherkaoui and Wilcock*, 1999] which have downflow zones that remain cold until the fluids enter the bottom boundary layer and with the common assumptions underlying single pass pipe models [e.g., *Lowell and Germanovich*, 2004]. It is however, compatible with the temperature distribution inferred from the study of the mineral assemblages found at different levels in oceanic crust [*Alt*, 1995]. For example, the initial stages of recharge up to a few hundreds of meters below the seafloor are characterized by oxidation, alkali and Mg fixation in the crust. These processes lead to alteration products such as celadonite, nontronite and saponite which form at temperatures up to ∼150°C. Deeper in the recharge zone, anhydrite forms at temperatures >150°C as basaltic calcium is added to the circulating fluids and the loss of magnesium from the circulating fluids occurs when chlorite forms at temperature >200°C.

[42] It has been argued that anhydrite precipitation can clog downflow pathways near the reaction zone so efficiently that black smoker activity cannot be maintained for periods exceeding 100 years unless recharge area are 10 to 100 times wider than discharge area [*Lowell and Yao*, 2002]. *Lowell and Yao* [2002] argue that, when recharge zones are broader, the lower specific mass flux (in kg/s/m^2) allows the 150°C isotherm to reach much higher levels in the crust. The region of the recharge area with temperatures >150°C is then larger and anhydrite precipitation occurs over a much greater vertical extent. The temperature structure in our models imply that anhydrite precipitation will not be limited to the deepest parts of the downflow zone even when recharge areas are only a few times wider than discharge areas. We infer that black smoker systems with relatively narrow recharge zones may not be as susceptible to clogging by anhydrite as *Lowell and Yao* [2002] infer. However, this inference has to be tempered by the fact that our models do not actually include anhydrite precipitation and the dynamical feedback between the permeability reduction and the convective flow are difficult to predict.

6. Conclusions

[43] In this paper we present two-dimensional numerical experiments to simulate hydrothermal circulation at mid-ocean ridges at high Rayleigh and Nusselt numbers. To avoid classical numerical issues such as the artificial diffusion of the temperature field or the development of nonphysical oscillatory behavior close to thermal fronts, we use the MPDATA technique devised by *Smolarkiewicz* [1984]. We solve the temperature equation using a classical upwind scheme which artificially diffuses the temperature field. We then estimate the artificial

diffusion and correct the solutions, iteratively. We benchmark our technique with previous studies that use constant fluid properties and the Boussinesq approximation and we then apply our models to hydrothermal circulation in mid-ocean ridges incorporating realistic fluid properties into the models. Our solutions for high Rayleigh/Nusselt number flow at mid-ocean ridges are reasonably consistent with those obtained recently with a different technique for a similar model configuration [*Coumou et al.*, 2006].

[44] Although our simulations describe very simplified geological configurations, they have important first-order implications for mid-ocean ridge hydrothermal systems:

[45] 1. For permeability $>\sim 10^{-15}$ m^2, corresponding to $Nu > \sim 13$, hydrothermal circulation is unsteady and heat extraction from the crust evolves from periodic to chaotic behavior.

[46] 2. The reaction zones of mid-ocean ridge hydrothermal systems are not steady state and temperatures oscillate substantially with the passage of thermal instabilities. This increases the volume of rock that is available to the reaction zone over time and may explain the stability of vent chemistry without having to invoke a model in which hydrothermal fluids continually penetrate downward into fresh rock.

[47] 3. Hydrothermal discharge can stop temporarily as zones of venting are dynamically replaced by zones of seawater recharge

[48] 4. A large portion of the downflow zone exceeds 150°C and therefore we infer that anhydrite precipitation will occur over a large range of depths and will not necessarily clog downflow pathways as has recently been inferred [*Lowell and Yao*, 2002].

[49] Future work should build upon these models by employing alternative numerical techniques to verify the results, considering more realistic permeability distributions, and investigating the effects of phase separation and segregation on the patterns of flow at high Rayleigh numbers.

Acknowledgments

[50] We thank Robert Lowell, Sebastian Geiger, and William Seyfried for their thorough reviews of earlier versions of this manuscript and Michel Rabinowicz and Arnaud Antkowiak for helpful discussions. Publication of this work was supported by a grant OCE-0243395 from the National Science Foundation.

References

Alt, J. C. (1995), Subseafloor processes in mid-ocean ridge hydrothermal systems, in *Seafloor Hydrothermal Systems: Physical, Chemical, Biological and Geological Interactions*, *Geophys. Monogr. Ser.*, vol. 91, edited by S. E. Humphris et al., pp. 85–114, AGU, Washington, D. C.

Anderko, A., and K. S. Pitzer (1993), Equation-of-state representation of phase equilibria and volumetric properties of the system NaCl-H_2O above 573 °K, *Geochim. Cosmochim. Acta*, *57*, 1657–1680.

Bell, J. B., G. R. Shubin, and J. A. Trangenstein (1986), A method for reducing numerical dispersion in two-phase back-oil reservoir simulation, *J. Comput. Phys.*, *65*, 71–106.

Bemis, K. G., R. P. Von Herzen, and M. J. Mottl (1993), Geothermal heat flux from hydrothermal plumes on the Juan de Fuca Ridge, *J. Geophys. Res.*, *98*, 6351–6366.

Bischoff, J. L., and R. J. Rosenbauer (1989), Salinity variations in submarine hydrothermal systems by layered double-diffusive convection, *J. Geol.*, *97*, 613–623.

Butterfield, D. A., and G. J. Massoth (1994), Geochemistry of North Cleft segment vent fluids: Temporal changes in chlorinity and their possible relation to recent volcanism, *J. Geophys. Res.*, *99*, 4951–4968.

Butterfield, D. A., W. E. Seyfried, and M. D. Lilley (2003), Composition and evolution of hydrothermal fluids, in *Energy and Mass Transfer in Submarine Hydrothermal Systems*, *Dahlem Workshop Rep.*, vol. 89, edited by P. E. Halbach et al., pp. 123–161, Free Univ. of Berlin, Berlin.

Butterfield, D. A., K. K. Roe, M. D. Lilley, J. A. Huber, J. A. Baross, R. W. Embley, and G. J. Massoth (2004), Mixing, reaction and microbial activity in the sub-seafloor revealed by temporal and spatial variation in diffuse flow vents at Axial Volcano, in *The Subseafloor Biosphere at Mid-Ocean Ridges*, *Geophys. Monogr. Ser.*, vol. 144, edited by W. S. D. Wilcock et al., pp. 269–290, AGU, Washington, D. C.

Caltagirone, J. P., and P. Fabrie (1989), Natural convection in a porous medium at high Rayleigh numbers, Part I—Darcy's Model, *Eur. J. Mech. B/Fluids*, *8*, 549–553.

Cherkaoui, A. S. M., and W. S. D. Wilcock (1999), Characteristics of high Rayleigh number two-dimensional convection in an open-top porous layer heated from below, *J. Fluid Mech.*, *394*, 241–260.

Cherkaoui, A. S. M., W. S. D. Wilcock, and E. T. Baker (1997), Thermal fluxes associated with the 1993 diking event on the CoAxial segment, Juan de Fuca Ridge: A model for the convective cooling of a dike, *J. Geophys. Res.*, *102*, 24,887–24,902.

Cherkaoui, A. S. M., W. S. D. Wilcock, R. A. Dunn, and D. R. Toomey (2003), A numerical model of hydrothermal cooling and crustal accretion at a fast spreading mid-ocean ridge, *Geochem. Geophys. Geosyst.*, *4*(9), 8616, doi:10.1029/2001GC000215.

Cooper, M. J., H. Elderfield, and A. Schultz (2000), Diffuse hydrothermal fluids from Lucky Strike hydrothermal vent field: Evidence for a shallow conductively heated system, *J. Geophys. Res.*, *105*, 19,369–19,376.

Corliss, J. B., et al. (1979), Submarine thermal springs on the Galapagos rift, *Science*, *203*, 1073–1083.

Coumou, D., T. Driesner, S. Geiger, C. A. Heinrich, and S. Matthäi (2006), The dynamics of mid-ocean ridge hydrothermal systems: Splitting plumes and fluctuating vent temperatures, *Earth. Planet. Sci. Lett.*, *245*, 218–231.

Dubuffet, F., M. Rabinowicz, and M. Monnereau (2000), Multiple scales in mantle convection, *Earth Planet. Sci. Lett.*, *178*, 351–366.

Durlofsky, L. J., B. Engquist, and S. Osher (1992), Triangle based adaptive stencils for the solution of hyperbolic conservation laws, *J. Comput. Phys.*, *98*, 64–73.

Fehn, U., and L. M. Cathles (1979), Hydrothermal convection at slow-spreading mid-ocean ridges, *Tectonophysics*, *55*, 239–260.

Fehn, U., K. E. Green, R. P. Von Herzen, and L. W. Cathles (1983), Numerical models for the hydrothermal field at the Galapagos spreading center, *J. Geophys. Res.*, *88*, 1033–1048.

Fontaine, F. J., and W. S. D. Wilcock (2006), Dynamics and storage of brine in mid-ocean ridge hydrothermal systems, *J. Geophys. Res.*, *111*, B06102, doi:10.1029/2005JB003866.

Fontaine, F. J., M. Rabinowicz, and J. Boulègue (2001), Permeability changes due to mineral diagenisis in fractured crust: Implications for hydrothermal circulation at mid-ocean ridges, *Earth Planet Sci. Lett.*, *184*, 407–425.

Fornberg, B. (1998), *A Practical Guide to Pseudo-spectral Methods*, Cambridge Univ. Press, Cambridge, U. K.

Geiger, S., S. Roberts, S. K. Matthäi, C. Zoppou, and A. Burri (2004), Combining finite element and finite volume methods for efficient multiphase flow simulations in highly heterogeneous and structurally complex geologic media, *Geofluids*, *4*, 284–299.

Geiger, S., T. Driesner, C. A. Heinrich, and S. K. Matthäi (2005), On the dynamics of NaCl-H_2O fluid convection in the Earth's crust, *J. Geophys. Res.*, *110*, B07101, doi:10.1029/2004JB003362.

Geiger, S., T. Driesner, C. A. Heinrich, and S. K. Matthäi (2006), Multiphase thermohaline convection in the Earth's crust: I. A new finite element–finite solution technique combined with a new equation of state for NaCl-H_2O, *Transp. Porous Media*, *36*, 399–434.

German, C. R., and J. Lin (2004), The thermal structure of the oceanic crust, ridge-spreading and hydrothermal circulation: How well do we understand their inter-connections?, in *Mid-Ocean Ridges: Hydrothermal Interactions Between the Lithosphere and Oceans*, *Geophys. Monogr. Ser.*, vol. 148, edited by C. R. German et al., pp. 1–18, AGU, Washington, D. C.

Gillis, K. M., K. Muehlenbachs, M. Stewart, T. Gleeson, and J. Karson (2001), Fluid flow patterns in fast spreading East Pacific Rise crust exposed at Hess Deep, *J. Geophys. Res.*, *106*, 26,311–26,330.

Graham, M. D., and P. H. Steen (1994), Plume formation and resonant bifurcations in porous-media convection, *J. Fluid Mech.*, *272*, 67–89.

Harten, A., B. Engquist, S. Osher, and S. R. Chakravarthy (1987), Uniformly high-order accurate essentially non-oscillatory schemes, III., *J. Comput. Phys.*, *71*, 231–303.

Henstock, T. J., A. W. Woods, and R. S. White (1993), The accretion of oceanic crust by episodic sill intrusion, *J. Geophys. Res.*, *98*, 4143–4162.

Hirth, G., J. Escartin, and J. Lin (1998), The rheology of the lower oceanic crust: Implications for lithospheric deformation at mid-ocean ridges, in *Faulting and Magmatism at Mid-Ocean Ridges*, *Geophys. Monogr. Ser.*, vol. 106, edited by W. R. Buck et al., pp. 291–303, AGU, Washington, D. C.

Humphris, S. E., and J. R. Cann (2000), Constraints on the energy and chemical balances of the modern TAG and ancient Cyprus seafloor sulfide deposits, *J. Geophys. Res.*, *105*, 28,477–28,488.

Jupp, T., and A. Schultz (2000), A thermodynamic explanation for black smoker temperatures, *Nature*, *403*, 880–883.

Kawada, Y., S. Yoshida, and S. Watanabe (2004), Numerical simulations of mid-ocean ridge hydrothermal circulation including the phase separation of seawater, *Earth Planets Space*, *56*, 193–215.

Kimura, S., G. Schubert, and J. M. Straus (1986), Route to chaos in porous-medium thermal convection, *J. Fluid. Mech.*, *116*, 305–324.

Kissling, W. M. (2005), Transport of three-phase hypersaline brines in porous media: Theory and code implementation, *Transp. Porous Media*, *61*, 25–44.

Lalou, C., J.-L. Reyss, E. Brichet, P. A. Rona, and G. Thompson (1995), Hydrothermal activity on a 105-year scale at a slow-spreading ridge, TAG hydrothermal field, Mid-Atlantic Ridge 26°N, *J. Geophys. Res.*, *100*, 17,855–17,862.

Lister, C. R. B. (1974), On the penetration of water into hot rock, *Geophys. J. R. Astron. Soc.*, *39*, 465–509.

Lister, C. R. B. (1983), The basic physics of water penetration into hot rocks, in *Hydrothermal Processes at Seafloor Spreading Center*, edited by P. A. Rona et al., pp. 141–168, Plenum, New York.

Lowell, R. P. (1991), Modeling continental and submarine hydrothermal systems, *Rev. Geophys.*, *29*, 457–477.

Lowell, R. P., and L. N. Germanovich (2004), Hydrothermal processes at mid-ocean ridges: Results from scale analysis and single-pass models, in *Mid-Ocean Ridges: Hydrothermal Interactions Between the Lithosphere and Oceans*, *Geophys. Monogr. Ser.*, vol. 148, edited by C. R. German et al., pp. 110–127, AGU, Washington, D. C.

Lowell, R. P., and Y. Yao (2002), Anhydrite precipitation and the extent of hydrothermal recharge zones at ocean ridge crests, *J. Geophys. Res.*, *107*(B9), 2183, doi:10.1029/2001JB001289.

Lowell, R. P., P. A. Rona, and R. P. Von Herzen (1995), Seafloor hydrothermal systems, *J. Geophys. Res.*, *100*, 327–352.

Manning, C. E., P. E. Weston, and K. I. Mahon (1996), Rapid high-temperature metamorphism of East Pacific Rise gabbros from Hess Deep, *Earth Planet. Sci. Lett.*, *144*, 123–132.

Macdonald, K. C., K. Becker, F. N. Spiess, and R. Ballard (1980), Hydrothermal heat flux of the "black smoker" vents on the East Pacific Rise, *Earth Planet. Sci. Lett.*, *48*, 1–7.

Meyer, C. A., R. B. McClintock, G. J. Silvestri, and R. C. Spencer Jr. (1993), *ASME Steam Table: Thermodynamic and Transport Properties of Steam*, Am. Soc. of Mech. Eng., New York.

Morgan, J. P., and Y. J. Chen (1993), The genesis of oceanic crust: Magma injection, hydrothermal circulation, and crustal flow, *J. Geophys. Res.*, *98*, 6283–6298.

Nehlig, P. (1994), Fracture and permeability analysis in magma-hydrothermal transition zones in the Samail ophiolite (Oman), *J. Geophys. Res.*, *99*, 589–602.

Pascoe, A. R., and J. R. Cann (1995), Modeling diffuse hydrothermal flow in black smoker vent fields, in *Hydrothermal Vents and Processes*, edited by L. M. Parsons et al., *Geol. Soc. Spec. Publ.*, *87*, 159–173.

Pitzer, K. S., J. C. Peiper, and R. H. Busey (1984), Thermodynamic properties of aqueous sodium chloride solutions, *J. Phys. Chem. Ref. Data*, *13*, 1–106.

Potter, R. W., II, and D. L. Brown (1977), The volumetric properties of aqueous sodium chloride solutions from 0° to 500°C at pressures up to 2000 bars based on a regression of available data in literature, *U. S. Geol. Surv. Bull.*, *1421–C*, 36 pp.

Rabinowicz, M., J. Boulègue, and P. Genthon (1998), Two- and three-dimensional modeling of hydrothermal convection

in the sedimented Middle Valley segment, Juan de Fuca Ridge, *J. Geophys. Res.*, *103*, 24,045–24,065.

Rabinowicz, M., J.-C. Sempéré, and P. Genthon (1999), Thermal convection in a vertical permeable slot: Implications for hydrothermal circulation along mid-ocean ridges, *J. Geophys. Res.*, *104*, 29,275–29,292.

Ribando, R. J., K. E. Torrance, and D. L. Turcotte (1976), Numerical models for hydrothermal circulation in the oceanic crust, *J. Geophys. Res.*, *81*, 3007–3012.

Rona, P. A., M. D. Hannington, C. V. Raman, G. Thompson, M. K. Tivey, S. E. Humphris, C. Lalou, and S. Petersen (1993), Active and relict sea-floor hydrothermal mineralization at the TAG hydrothermal field, Mid-Atlantic Ridge, *Econ. Geol.*, *88*, 1989–2017.

Rosenberg, N. D., and F. J. Spera (1990), Role of anisotropic and/or layered permeability in hydrothermal convection, *Geophys. Res. Lett.*, *17*, 235–238.

Rosenberg, N. D., F. J. Spera, and R. M. Haymon (1993), The relationship between flow and permeability field in seafloor hydrothermal systems, *Earth Planet. Sci. Lett.*, *116*, 135–153.

Schoofs, S., and U. Hansen (2000), Depletion of a brine layer at the base of ridge-crest hydrothermal systems, *Earth Planet Sci. Lett.*, *180*, 341–353.

Schultz, A., J. R. Delaney, and R. E. McDuff (1992), On the partitioning of heat flux between diffuse and point source seafloor venting, *J. Geophys. Res.*, *97*, 12,299–12,314.

Seyfried, W. E., Jr., and K. Ding (1995), Phase equilibria in subseafloor hydrothermal systems: A review of the role of redox, temperature, pH and dissolved Cl on the chemistry of hot spring fluids at mid-ocean ridges, in *Seafloor Hydrothermal Systems*, *Geophys. Monogr. Ser.*, vol. 91, edited by S. E. Humphris et al., pp. 249–272, AGU, Washington, D. C.

Seyfried, W. E., Jr., K. Ding, and M. E. Berndt (1991), Phase equilibria constraints on the chemistry of hot spring fluids at mid-ocean ridges, *Geochem. Cosmochem. Acta*, *55*, 3559–3580.

Singh, S. C., J. S. Collier, A. J. Harding, G. M. Kent, and J. A. Orcutt (1999), Seismic evidence for a hydrothermal layer above the solid roof of the axial magma chamber at the southern East Pacific Rise, *Geology*, *27*, 219–222.

Singh, S. C., et al. (2006), Discovery of a magma chamber and faults beneath a Mid-Atlantic Ridge hydrothermal field, *Nature*, *442*, 1029–1032.

Smolarkiewicz, P. K. (1984), A fully multidimensional positive definite advection transport algorithm with small implicit diffusion, *J. Comput. Phys.*, *54*, 325–362.

Smolarkiewicz, P. K., and T. L. Clark (1986), The multidimensional positive definite advection transport algorithm: Further development and applications, *J. Comput. Phys.*, *67*, 396–438.

Steen, P. H., and C. K. Aidun (1988), Time-periodic convection in porous media: Transition mechanism, *J. Fluid. Mech.*, *196*, 263–290.

Tivey, M. K., S. E. Humphris, G. Thompson, M. D. Hannington, and P. A. Rona (1995), Deducing patterns of fluid flow and mixing within the TAG active hydrothermal mound using mineralogical and geochemical data, *J. Geophys. Res.*, *100*, 12,527–12,555.

Toomey, D. R., S. C. Solomon, and G. M. Purdy (1994), Tomographic imaging of the shallow crustal structure of the East Pacific Rise at 9°30′N, *J. Geophys. Res.*, *99*, 24,135–24,157.

Travis, B. J., D. R. Janecky, and N. D. Rosenberg (1991), Three-dimensional simulation of hydrothermal circulation at mid-ocean ridges, *Geophys. Res. Lett.*, *18*, 1441–1444.

Veirs, S. R., R. E. McDuff, and F. R. Stahr (2006), Magnitude and variance of near-bottom horizontal heat flux at the Main Endeavour hydrothermal vent field, *Geochem. Geophys. Geosyst.*, *7*, Q02004, doi:10.1029/2005GC000952.

Von Damm, K. L. (1995), Control on the chemistry and temporal variability of seafloor hydrothermal fluids, in *Seafloor Hydrothermal Systems: Physical, Chemical, Biological and Geological Interactions*, *Geophys. Monogr. Ser.*, vol. 91, edited by S. E. Humphris et al., pp. 222–247, AGU, Washington, D. C.

Von Damm, K. L. (2004), Evolution of the hydrothermal system at East Pacific Rise 9°50′N: Geochemical evidence for changes in the upper oceanic crust, in *Mid-Ocean Ridges: Hydrothermal Interactions Between the Lithosphere and Oceans*, *Geophys. Monogr. Ser.*, vol. 148, edited by C. R. German et al., pp. 285–304, AGU, Washington, D. C.

Von Damm, K. L., C. M. Parker, R. A. Zierenberg, M. D. Lilley, E. J. Olson, D. A. Clague, and J. S. McClain (2005), The Escanaba Trough, Gorda Ridge hydrothermal system, temporal stability and sub-seafloor complexity, *Geochim. Cosmochim. Acta*, *69*, 4971–4984.

White, S. N., S. E. Humphris, and M. C. Kleinrock (1998), New observations on the distribution of past and present hydrothermal activity in the TAG area of the Mid-Atlantic Ridge (26°08′N), *Mar. Geophys. Res.*, *20*, 41–56.

Wilcock, W. S. D. (1997), A model for the formation of transient event plumes above mid-ocean ridge hydrothermal systems, *J. Geophys. Res.*, *102*, 12,109–12,122.

Wilcock, W. S. D. (1998), Cellular convection models of mid-ocean ridge hydrothermal circulation and the temperatures of black smoker fluids, *J. Geophys. Res.*, *103*, 2585–2596.

Wilcock, W. S. D., and J. R. Delaney (1996), Mid-ocean ridge sulfide deposits: Evidence for heat extraction from magma chambers or cracking fronts?, *Earth Planet. Sci. Lett.*, *149*, 49–64.

Wilcock, W. S. D., and A. T. Fisher (2004), Geophysical constraints on the subseafloor environment near mid-ocean ridges, in *The Subseafloor Biosphere at Mid-Ocean Ridges*, *Geophys. Monogr. Ser.*, vol. 144, edited by W. S. D. Wilcock et al., pp. 51–74, AGU, Washington, D. C.

Williams, D. L., R. P. von Herzen, J. G. Sclater, and R. N. Anderson (1974), The Galapagos spreading center: Lithospheric cooling and hydrothermal circulation, *Geophys. J. R. Astron. Soc.*, *38*, 587–608.

Xu, W., and R. P. Lowell (2000), Sub-critical two-phase seawater convection near a dike, *Earth. Planet. Sci. Lett.*, *174*, 385–396.

Zalesak, S. T. (1979), Fully multidimensional flux-corrected transport algorithms for fluids, *J. Comput. Phys.*, *31*, 335–362.

Zonenshain, L. P., M. I. Kuzmin, A. P. Lisitsyn, Y. A. Bogdanov, and B. W. Baranov (1989), Tectonics of the Mid-Atlantic Rift valley between the TAG and MARK areas (26–24°N): Evidence for vertical tectonism, *Tectonophysics*, *159*, 1–23.